Short Baseline Phase Delay Interferometry

C. D. Edwards
Tracking Systems and Applications Section

The high precision of the phase delay data type allows angular navigation accuracy on relatively short baselines to compete with the angular accuracy achieved with long baseline group delay measurements. Differential phase delay observations of close quasar pairs on both a 5.9-km baseline (DSS 12–DSS 13) and a 253-km baseline (DSS 13–Owens Valley Radio Observatory) have been performed to study the potential navigational precision and accuracy of short baseline interferometry. As a first step toward demonstration of a connected element system at Goldstone, the DSS 12–DSS 13 baseline was operated coherently, distributing a common frequency reference via a recently installed fiber optic cable. The observed phase delay residuals of about 10 psec or less on both baselines appear to be dominated by short term troposphere fluctuations, and correspond to navigational accuracies of well below 50 nrad for the 253-km baseline. Additional experiments will be required to probe the full range of systematic errors.

I. Introduction

Very long baseline interferometry (VLBI) currently provides high accuracy angular spacecraft navigation for the Deep Space Network (DSN). Relative to the highly stable inertial reference frame defined by extragalactic radio sources, the DSN Block I VLBI system can provide spacecraft angular position measurements with accuracy better than 50 nrad, using intercontinental baselines of lengths up to 10,000 km. The work reported here is an investigation of the extent to which interferometric observations on much shorter baselines can provide competitive results. In terms of ease of operation, reliability, observing bandwidth, and faster access to navigational data, short baseline interferometry offers a number of advantages over intercontinental VLBI. After briefly reviewing interferometry and the different interferometric data types, the advantages of short baselines and connected element interferometry (CEI) will be examined. Recent experimental results for baselines of 5.9 and 253 km will be presented, indicating the current level of position accuracy to be 1–5 mm. Finally, future plans for evaluating the potential of CEI will be considered.

II. Interferometric Phase and Group Delay Data Types

In interferometry, we are essentially interested in measuring the geometric delay representing the difference in arrival times of a signal wavefront at two separate antennas. Letting $\mathbf{B}$ be the baseline between the two stations and $\hat{\mathbf{s}}$ the unit vector in the direction of the radio source, the geometric delay is simply:

$$\tau = \frac{1}{c}\mathbf{B}\cdot\hat{\mathbf{s}}$$

$$= \frac{1}{c}B\cos\theta$$

where c is the speed of light and θ is the angle between the baseline vector and the source direction. This geometric delay, coupled with accurate knowledge of the baseline length and orientation, provides a precise angular position for the radio source. In terms of the delay error $\sigma(\tau)$, the angular position accuracy is:

$$\sigma(\theta) = \frac{c\sigma(\tau)}{B|\sin\theta|}$$

Angular navigation can be improved either by increasing the baseline length or by reducing the delay error.

To measure the delay τ, the signals from the two antennas are brought together and correlated. (See [1], for example.) The primary output of this correlation process is the interferometric phase, which, in the absence of unmodeled errors, is a measurement of the geometric delay in units of the observing wavelength. In terms of the interferometric phase ϕ, the phase delay τ_ϕ is simply:

$$\tau_\phi = \frac{\phi}{\nu_{RF}}$$

where ν_{RF} is the RF observing frequency. The cycle ambiguity associated with the phase determination corresponds to a delay ambiguity of $1/\nu_{RF}$. The fractional number of wavelengths in the geometric delay is measured very accurately, but the integral number is unknown. Therefore, unless *a priori* knowledge of the geometric delay is much better than a cycle of RF phase, and all error sources can be controlled to much better than an RF cycle, the high precision of the phase delay data type cannot be utilized.

In those cases where the *a priori* delay knowledge is not accurate enough to resolve the RF cycle ambiguity, one can instead measure the slope of phase *vs.* frequency to obtain the less precise group delay. In practice, the bandwidth synthesis (BWS) technique is used [2] in which the interferometric phase is observed at two (or more) nearby RF frequencies, yielding a measurement of the group delay τ_{BWS}:

$$\tau_{BWS} = \frac{\phi_1 - \phi_2}{\Delta\nu}$$

where $\Delta\nu$ is the difference of the two observing frequencies. The group delay still has an ambiguity associated with it, of size $1/\Delta\nu$, but since typically $\Delta\nu \ll \nu_{RF}$, the BWS ambiguity is usually much larger than the phase delay ambiguity, and hence much less stringent *a priori* delay knowledge is required to resolve the group delay ambiguity. The increased delay ambiguity, however, is accompanied by a reduced delay precision.

An example will put this in perspective. Consider an interferometric observation with a signal-to-noise ratio SNR = 10. Let the RF observing frequency be ν_{RF} = 8.4 GHz, with observations at two channels separated by $\Delta\nu$ = 40 MHz, typical values for the DSN Block 0 and Block I VLBI systems. Table 1 summarizes the resulting delay precision and ambiguity for both the phase and group delay data types. The phase delay precision of 2 psec is over two orders of magnitude smaller than the 560-psec precision of the group delay. However, the phase delay ambiguity of 120 psec is also over two orders of magnitude smaller than the group delay ambiguity of 25 nsec.

In typical intercontinental VLBI observations, a number of error sources cause the *a priori* model delay error to be on the order of an RF cycle or larger, preventing the use of the high precision phase delay data type. As a result, the group delay has routinely been used to supply delay estimates on long baselines for spacecraft navigation.

On short baselines, however, cancellation of the effects of many of these error sources between the two stations reduces the *a priori* delay uncertainty to well below an RF cycle, enabling phase connection. The dominant delay error sources on intercontinental baselines include uncertainties in the zenith components of the troposphere and ionosphere, as well as angular uncertainties in the *a priori* source position and baseline orientation which produce delay errors proportional to baseline length. For baselines of a few hundred kilometers or less, the delay uncertainty corresponding to angular errors in source position and baseline orientation becomes much less than an RF cycle. Also, partial cancellation of the effects of the troposphere and ionosphere occurs on these shorter baselines, due both to spatial correlations in these media and to the fact that on shorter baselines, both stations are observing at roughly the same elevation angle. On sufficiently short baselines, the delay error budget will be dominated by baseline length-independent errors such as instrumental stability and antenna flexure, and by rapid fluctuations in the density of water vapor over each antenna, on a scale size smaller than the antenna separation.

Reduction of delay errors can also be achieved by limiting observations to sources within a small region of the sky. Delay errors which vary slowly over the sky will cancel to a large extent between observations of angularly close sources. (This strategy is used in Delta Differential One-way Range [Delta-DOR] navigation observations, in which a spacecraft's angular position is measured with respect to a nearby quasar.) By combining close source separations with short baselines, delay errors can be substantially reduced through cancellation, fur-

ther enabling phase ambiguity resolution. Of the two phase connection experiments reported here, one corresponds to a baseline length of 5.7 km with source separations of 10–20 degrees on the sky, while the other corresponds to a 253-km baseline with roughly 2-degree source separations.

III. Advantages of Short Baseline Interferometry

The use of intercontinental baselines is motivated by the fact that, for a given interferometric delay accuracy, the resulting angular accuracy is inversely proportional to baseline length. As we have seen, however, use of the more precise phase data type on shorter baselines can provide results competitive with group delay accuracy on longer baselines. In addition, a number of operational advantages result from observing on shorter baselines.

For intercontinental baselines, only a limited portion of the sky is simultaneously visible from both antennas. For example, on the Goldstone–Canberra DSN baseline, with an elevation angle cutoff of 6 deg, the solid angle visible from both complexes at any given time is only 32 percent of 2π sr. On the other hand, for observations within a single DSN complex, with the same 6-deg elevation cutoff the instantaneous mutual visibility approaches 90 percent of 2π sr. This would significantly relax scheduling constraints for tracking during critical mission periods.

A related problem with intercontinental baselines is that observations must often be made with one or both stations at very low elevation angles, increasing the effects of the troposphere. As an example, consider intracomplex Goldstone observations of a source at –23-deg declination. At transit, the source will be at an elevation angle of 31.7 deg, corresponding to a total pathlength through the atmosphere, summed over both antennas, of 3.8 atmospheres. For the Goldstone–Canberra intercontinental baseline, the minimum total pathlength is only slightly larger, at 4.2 atmospheres, but for the Goldstone–Madrid baseline, the minimum total pathlength is 15.0 atmospheres. For those scenarios in which troposphere errors are a dominant part of the error budget, the capability of observing at higher elevation angles could significantly improve navigational accuracy.

The possibility of using the phase delay observable on shorter baselines also reduces the impact of instrumental phase uncertainties in the observing bandpass. For a differential spacecraft–quasar observation, the phase of the spacecraft tone will be affected by instrumental phase errors at the ground stations only at the tone frequency in the observing bandpass, whereas the phase of the broadband quasar signal is subjected to the average of the instrumental phase error across the observing bandpass. Any phase ripple across the bandpass will not cancel in the spacecraft–quasar difference and will corrupt the final navigational observable. This can produce a significant delay error in the group delay, equal to the size of the phase error divided by the spanned bandwidth. For example, with an uncalibrated phase ripple of 2 deg across the observing bandpass and a spanned bandwidth of 40 MHz, the resulting error in the group delay would be $\sqrt{2} \times (0.006 \text{ cyc})/(40 \text{ MHz})$, or about 200 psec. For the phase delay data type, however, the effect is just the phase error divided by the RF observing frequency. Thus at 8.4 GHz, the 2-deg phase ripple would only induce an error of 0.7 psec.

For baseline lengths of a few tens of kilometers or less, the observing stations can be directly connected by fiber optic cables, allowing the observed signals to be transported to a central correlator facility and processed in real time. In addition to decreasing the turnaround time for navigational data, real-time cross-correlation would improve reliability by providing verification of the data integrity, revealing any experimental configuration errors at the time of observation rather than hours or days later. The fiber optic links also enable distribution of a common frequency reference to the observing stations, eliminating the requirement for separate clocks and the need to solve for a clock rate offset between stations.

An additional advantage of real-time correlation is that data would not have to be recorded on tape, but would rather be routed directly to the correlator for processing. Eliminating the need for data recording would increase efficiency, eliminate costs for tapes and tape shipping, and greatly reduce the manpower required for correlation processing. With the burden of actually recording the observed signals removed, much larger observation bandpasses and consequent data rates could be supported, leading to improved signal-to-noise for the broadband quasar observations. This improved sensitivity could allow observation of weaker radio sources, increasing the density of the source catalog, and could shorten observing times for current radio sources.

Finally, it should be noted that the phase delay spacecraft measurement is a narrow band technique. The phase delay is determined from data at a single frequency, as opposed to the group delay, which requires observations at several frequencies. Just a single carrier wave spacecraft tone is required, rather than a set of tones with tens or hundreds of MHz separation. Charged particle calibration would still necessitate dual-band data, but again, only one tone at each band would be required, rather than several. Quasar observations will still require finite bandwidth, since the quasar cross-correlation SNR scales inversely with the square root of the recorded bandwidth. However, the large spanned bandwidths used in BWS are not

required. The data presented in this article were recorded with single 2-MHz bandpasses at 2.3 and 8.4 GHz.

IV. Goldstone Intracomplex Phase Delay Observations

A. Initial Tests of Fiber Optic Link

As a first step toward CEI at Goldstone, and to support a number of other intracomplex communication needs, four multi-mode and two single-mode fiber optic cables were installed between DSS 12 and DSS 13 in 1986. The single-mode fibers each offer over 1 GHz of bandwidth, and could eventually be used to transmit data to a central correlator facility. Currently the single-mode fiber is being used not for data transfer, but rather for transfer of a frequency reference from DSS 13 to DSS 12, enabling both stations to be operated coherently.

The first interferometry experiments using the fiber optic link between DSS 12 and DSS 13 were completed in August and September 1986. The fiber optic link was used to reference the local oscillators at both stations to the hydrogen maser frequency reference at DSS 13. The goal of these experiments was to verify the coherent operation of the two stations by successfully finding interferometric fringes, and secondly, to characterize the stability of the link by examining the phase residuals for individual quasar scans. Observations of a number of bright radio sources were made at 2.3 and 8.4 GHz, and a 2-MHz bandwidth at each frequency was translated to baseband, single-bit sampled, time-tagged, and recorded on videotape, using the Block 0 VLBI system. The experimental configuration is summarized in Fig. 1.

Figure 2 shows the Allan standard deviation of the phase residuals for a single 10-minute scan of the bright source 3C 84. At τ = 64 sec, the Allan standard deviation $\sigma_y(\tau) = 4.5 \times 10^{-14}$. Also indicated in the figure is the expected range of stability due to troposphere fluctuations, based on a calculation using the stochastic model of Treuhaft and Lanyi [3]. Instabilities in the VLBI instrumentation may also contribute at about this level or slightly lower.[1] The agreement indicates that wet troposphere fluctuations and perhaps station instrumental instabilities can account for the observed phase fluctuations, suggesting that the stability of the fiber optic link for frequency transfer is below this level. Independent measurements of the round trip link stability by members of the Time and Frequency Systems Research Group at JPL yielded an Allan standard deviation of 1.5×10^{-15} at τ = 1000 sec, and below 10^{-14} at τ = 64 sec [4], again indicating that the fiber optic link is more stable than the expected level of wet troposphere fluctuations.

B. Phase Connection Results for Clusters of Sources

To demonstrate phase connection on short baselines, interferometric observations of a number of extragalactic radio sources were made between DSS 12 and DSS 13 on March 21, 1987. Data were recorded at 2.3 and 8.4 GHz using the same Block 0 configuration as described above. Most of the observations were 3 minutes long and were grouped into clusters of 8–10 scans. The goal of this experiment was to determine the reliability of phase ambiguity resolution, and quantify limiting error sources, by examining the final RMS scatter of phase delay residuals within each cluster.

Each cluster consisted of repeated observations of two or three angularly close radio sources. Separation angles for sources within a cluster ranged from 10 to 20 deg, representative of typical spacecraft–quasar angular separations in current Delta-DOR navigation observations. As mentioned earlier, limiting observations to angularly close sources leads to significant cancellation of many geometric and propagation media error sources, thereby decreasing the relative *a priori* model delay errors between sources and increasing the likelihood of successful phase connection.

The data were correlated off-line at the Caltech–JPL Block 0 Correlator, yielding phase measurements for each scan at both 2.3 and 8.4 GHz. Calibration tones embedded in the recorded bandpasses were also extracted, and the resulting instrumental phase variations at each station were removed from the phases for the radio sources. Based on the best available *a priori* knowledge of the positions of the radio sources and the station locations for DSS 12 and DSS 13, a model delay was calculated for each scan, and the residual delay difference between the observed phase delay and this model delay was calculated. These relative phases were then examined to correct the RF cycle ambiguities for these scans. The phase ambiguity of each scan was adjusted so that its residual delay was within half an ambiguity of the residual delay for the preceding scan. Finally, S/X ionosphere calibration was performed by forming the linear combination of 2.3- and 8.4-GHz observations which eliminated the dispersive effects of the ionosphere.

At this point in the analysis, the dominant uncertainty in the phase delay model is an unknown relative phase between the local oscillator chains at the two stations, attributable to phase uncertainties in the frequency transfer between stations and uncalibrated portions of the signal chain (e.g., the path between the antenna feed horn and the injection port for the phase calibration tones). This phase uncertainty manifests

[1] C. D. Edwards, IOM 335.4-558 to Tracking Systems and Applications Section (internal document), Jet Propulsion Laboratory, Pasadena, California, January 1986.

itself as a clock epoch offset between the two stations. Standard VLBI analysis routinely includes a clock term in the delay model to characterize the different clock behavior at the two stations. In addition to a constant clock epoch offset, one must typically include a linear term and sometimes a quadratic term to characterize frequency offsets and drifts between the clocks at the two sites. For this experiment, however, both stations were operated coherently, meaning that only the constant clock epoch term was required.

A weighted least-squares fit was used to adjust the final delay model to the observed phase delays. The DSS 12 station location and the differential zenith troposphere between stations were adjusted. In addition, a constant clock offset was estimated for each cluster of scans. The estimation of a separate clock epoch for each cluster means that the phase is only being connected between sources within a cluster. This makes the solution less sensitive to errors in station location, or errors which vary slowly over the sky, such as antenna deformation. The multiple clock epoch estimates will also tend to compensate for any slow, long term uncalibrated phase drifts between the instrumentation at the two stations. The shift in the DSS 12 station location, relative to the *a priori* location, was $\Delta x = -10 \pm 6$ mm, $\Delta y = 8 \pm 5$ mm, and $\Delta z = 1 \pm 7$ mm, while the differential troposphere adjustment was 0 ± 1 mm.

The final S/X delay residuals are plotted in Fig. 3 against UT of the observation. The clusters are separated by dashed vertical lines, with a size of 120 psec, or one cycle of phase at 8.4 GHz. The scatter of the data is much smaller than this ambiguity size, indicating the reliability of the phase ambiguity resolution. The statistical errors on the individual data points, based on signal-to-noise considerations, were below 1 psec for nearly all the scans. The actual size of the limiting systematic errors is reflected in the scatter of the repeated observations within a cluster. The RMS scatter of the residual delays for each cluster ranges from 2.8 psec up to 15.7 psec. It is interesting to note that the largest scatter is obtained for the lowest elevation data: the observations of DW 1335-12 and OP-192 in the third data cluster, for which the RMS delay scatter is 15.7 psec, were made at elevations of 8–20 deg. Aside from one scan in the final cluster, all other observations were made at elevations of 35–75 deg. The combined RMS delay residual for all 37 observations is 9.1 psec. While the sources of the limiting systematic errors are not fully known, the model of [3] suggests that troposphere fluctuations can account for much of the observed scatter. Table 2 summarizes these results. It should be kept in mind that the only parameters estimated in fitting the data were DSS 12 station location, differential troposphere delay, and the clock epoch offsets for each cluster of observations; the rest of the delay model, including the radio source positions, were fixed at their best *a priori* values.

(As a further test of the robustness of the phase connection solution, an additional solution was made adjusting only the clock epoch parameters; the station location and troposphere values were fixed at their *a priori* values. Similar results were obtained, with the combined RMS delay scatter increasing only slightly to 10.7 psec.)

V. Phase Connection Between Goldstone and Owens Valley

As encouraging as these results on the DSS 12–DSS 13 baseline are, they do not translate into very accurate angular navigation. Even with an optimal source–baseline geometry, 10-psec delay accuracy on a 5.9-km baseline only provides roughly 600-nrad angular position accuracy. Competing with intercontinental capabilities will require improved delay accuracy, longer baselines, or a combination of both.

To investigate the potential for phase connection on longer baselines, VLBI observations were made on the 253-km baseline between DSS 13 and the 40-meter telescope at Owens Valley Radio Observatory (OVRO) on May 20, 1986. The primary difference between these observations and the DSS 12–DSS 13 observations involves clocks: for the DSS 13–OVRO experiment, each station was referenced to its own hydrogen maser frequency standard, as opposed to the DSS 12–DSS 13 experiment for which the Goldstone fiber optic link was used to operate both stations coherently. Other than that, most experimental details were the same. Block 0 VLBI recording systems were used and correlation was again performed off-line at the Caltech/JPL Block 0 Correlator.

Observations were made of two pairs of angularly close radio sources: GC 1633+38 and 3C 345, which are separated by 2.25 deg, and 3C 371 and 1749+701, with a separation angle of 1.59 deg. These separation angles are considerably smaller than the 10–20 deg separations of the sources within the clusters used in the DSS 12–DSS 13 observations. As a first attempt at phase connection on this baseline, the smaller separation angles were chosen to help compensate for geometric error sources which depend on both baseline length and source separation. (For example, according to the model of [3], the RMS differential zenith troposphere delay on a 5.9-km baseline is only about 0.5 cm; for 253 km it rises to over 2 cm. Reducing source separations will reduce the differential effect of this error source.) Future experiments will attempt phase connection for larger source separations, using water vapor radiometers to calibrate the troposphere at each station.

As before, residual phase delays were formed by differencing the observed interferometric phase delay and a model

delay based on *a priori* values of station locations, source positions, earth orientation, zenith troposphere delays, etc. The dominant effect in these phase delay residuals is the clock behavior. However, because independent clocks were used at DSS 13 and OVRO, the clock modeling is more complicated for this experiment than for the DSS 12–DSS 13 fiber optic link experiment. The separate clocks will induce an unknown phase rate (of order 1 psec/sec) corresponding to a frequency offset between the two clocks, in addition to stochastic instabilities in each clock. To make use of the observed phase delays for the individual scans, we would have to model the relative behavior of the two clocks as a piecewise linear or quadratic function over the full experiment. To simplify the analysis and reduce the need to accurately model the clock behavior over long time periods, individual observations were combined to form differential observables for which the clock behavior drops out, as described below.

For a given quasar pair, a sequential triplet of observations, first of source A, then source B, and back to source A, was selected. Individual scans were 5 minutes in length, and each A-B-A sequence lasted from 16 to 32 minutes, depending on details of the observing schedule. The relative phases for the two observations of source A were adjusted based on the observed phase rates for those scans. (More explicitly, for the two observations of source A, a predicted phase difference was obtained based on the average of the observed phase rates and the time difference between observations. The relative phase ambiguities of the two source A observations were than adjusted to bring the actual phase difference to within half an ambiguity of this predicted phase difference.) These two phase delay observations of source A were then used to solve for a linear clock, and this linear clock was interpolated to the time of observation for source B. The phase ambiguity of source B was then adjusted to be within half a cycle of this interpolated clock term. Finally, the differential observable was then formed by subtracting the interpolated clock term from the observed phase delay residual for source B. It is worth noting that, in addition to a linear clock term, any other error sources which are constant or vary linearly with time over the A-B-A observing sequence will also be removed by this technique.

Four such differential observables were formed for each of the two quasar pairs, representing a total of 24 individual radio source observations. The residual differential delays are plotted in Fig. 4 as a function of observation epoch, and the scale of the 8.4-GHz delay ambiguity is indicated. The RMS residual scatter of the four observations of the differential delay between GC 1633+38/3C 345 was 8.9 psec. For 3C 371/1749+701, the RMS scatter was 3.1 psec. The observed RMS scatter is consistent with the expected level of temporal troposphere fluctuations on the 1000-sec time scale associated with individual A-B-A sequences, according to the model of [3].

For the small source separations used here, and given the fact that the observations were all above 45-deg elevation, the static troposphere error due to uncertainty in the zenith delay at each site is expected to be smaller than this fluctuating component. This suggests that phase connection may be possible on this baseline for much larger source separations, particularly if the length of the observing sequences can be shortened. Once again, the fact that the RMS of the residuals is much smaller than the delay ambiguity indicates that the phase has been correctly connected between the source pairs within each linear combination.

For this experiment, no parameters have been estimated. Forming the differential observables eliminates the need to solve for any clock parameters. The close proximity of the sources within each pair makes the differential delay quite insensitive to errors in station location or differential troposphere delay. With 2-deg source separation, for example, a 1-cm station location error would only affect the differential delay at the level of 1.2 psec or less, depending on the relative baseline–source geometry. Accurate *a priori* station locations and zenith troposphere delays would become more important for larger source separations. Table 3 summarizes the results of the DSS 13–OVRO data.

VI. Discussion and Future Plans

It is encouraging that the delay residuals for the 253-km baseline are of roughly the same size as for the 5.9-km baseline. Although the angular source separations were quite small for the DSS 13–OVRO data, the baseline was over 40 times larger. The delay uncertainties of 3–15 psec correspond to a path length uncertainty of 1–5 mm. On the DSS 13–OVRO baseline a 1-cm delay error would correspond to about a 50-nrad angular accuracy for an orientation of 45 deg between the baseline vector and source direction. Based on the very limited amount of data presented here, it is premature to try to estimate a current angular accuracy; nevertheless, the data suggest that systematic errors on differential observations of nearby sources may be well under 1 cm, even for baseline lengths of several hundred kilometers. If differential errors could be reduced to the 1-mm (3-psec) level, differential position accuracies of 50–100 nrad could be obtained on the 21.6-km Goldstone intracomplex baseline between DSS 13 and DSS 14.

Further short baseline phase delay experiments will be required to isolate the dominant error sources and understand their dependence on baseline length, source separation, and observing strategy. Repeated observations of source pairs over many experiments will more fully sample the range of possible systematic errors, providing a more reliable determination of the potential navigational accuracy.

The high precision of the phase delay data type should help in identifying and characterizing the various systematic errors. It may be possible to parameterize and remove certain deterministic errors, such as gravity-induced antenna deformations, if the high precision phase data can reveal the signature of the error in the delay residuals. Stochastic errors such as instrumental phase drifts or wet troposphere fluctuations will require improved calibration techniques. Reliable instrumental phase calibrations and line-of-sight water vapor radiometry will almost certainly be required to reduce differential errors to the 1-mm level for source separations of 10–20 deg.

VII. Summary

Current intercontinental spacecraft navigation makes use of the group data type. The considerably more accurate phase delay data type is not used due to problems resolving the associated cycle ambiguities. On shorter baselines of tens or even hundreds of kilometers, however, phase connection should be possible for reasonable source separations. Using the higher accuracy phase delay data type, short baseline navigation accuracy is competitive with long baseline group delay results. In addition, there are a number of advantages for short baseline and connected element observations over intercontinental VLBI in terms of reliability, efficiency, and visibility.

Frequency transfer over a fiber optic cable enables coherent operation of the 5.9-km baseline between DSS 12 and DSS 13. Stability analysis of phase residuals for single source observations on this baseline indicates that tropospheric fluctuations dominate any instabilities in the fiber optic link frequency transfer. Repeated measurements of clusters of angularly close quasars, with separation angles of 10–20 deg, yield an RMS phase delay scatter of 10 psec, or 3 mm.

Successful phase connection was also achieved on the 253-km baseline between DSS 13 and OVRO, albeit for closer source separation angles of about 2 deg. Due to the use of two independent frequency standards on this longer baseline, linear combinations were formed for observations of neighboring radio sources, eliminating the effect of clock epoch and clock rate offsets. The RMS scatter of the differential measurements was below 10 psec. A delay accuracy of 30 psec, or 1 cm, on this baseline would yield a differential position accuracy of 50 nrad.

A large number of experiments will need to be carried out in the future to better understand the phase delay error budget, and the dependence of various errors on baseline length and source separation.

References

[1] J. B. Thomas, *An Analysis of Radio Interferometry with the Block 0 System*, JPL Publication 81-49, Jet Propulsion Laboratory, Pasadena, California, December 15, 1981.

[2] A. E. E. Rogers, "Very Long Baseline Interferometry with Large Effective Bandwidth for Phase-delay Measurements," *Radio Sci.*, vol. 5, pp. 1239–1247, October 1970.

[3] R. N. Treuhaft and G. E. Lanyi, "The Effect of the Dynamic Wet Troposphere on Radio Interferometric Measurements," *Radio Sci.*, vol. 22, pp. 251–265, March–April 1987.

[4] G. Lutes and A. Kirk, "Reference Frequency Transmission Over Optical Fibers," *TDA Progress Report 42-87*, vol. July–September, Jet Propulsion Laboratory, Pasadena, California, pp. 1–9, November 15, 1986.

Table 1. Properties of phase delay vs. group delay

	Phase delay	Group delay (BWS)
τ	$\frac{\phi}{\nu_{RF}}$	$\frac{\phi_1 - \phi_2}{\nu_1 - \nu_2}$
σ_τ	$\frac{\sigma_\phi}{\nu_{RF}}$	$\frac{\sqrt{2}\sigma_\phi}{\nu_1 - \nu_2}$
	(=2 psec)	(=560 psec)
Ambiguity	$\frac{1}{\nu_{RF}}$	$\frac{1}{\nu_1 - \nu_2}$
	(=120 psec)	(=25 × 10^3 psec)

Numerical values are for the case SNR = 10, ν_{RF} = 8.4 GHz, and $\nu_1 - \nu_2$ = 40 MHz.

Table 2. Intracomplex Goldstone phase delay results

Section	Sources	Separation angle	Number of observations	RMS delay
1	3C 84 NRAO 140 OE 400	6.4–16.2 deg	10	3.1 psec
2	OJ 287 P 0735+17	18.3 deg	8	7.9
3	DW 1335–12 OP–192	5.4 deg	8	15.7
4	OJ 287 P 0735+17	18.3 deg	8	7.6
5	P 1144–379 DW 1335–12 OP–192	5.4–36.5 deg	3	2.8
		Total	37	9.1 psec

DSS 12–DSS 13 baseline length: 5.9 km.
Fiber optic link used to transfer DSS 13 H-maser reference to DSS 12.

Table 3. DSS 13–OVRO phase delay results

Section	Sources	Separation angle	Number of observations	RMS delay
1	GC 1633+38 3C 345	2.25 deg	4 differential	8.9 psec
2	3C 371 1749+701	1.59 deg	4 differential	3.1
		Total	8 differential	6.7 psec

DSS 13–OVRO baseline length: 253 km.

Differential delay observable is formed from A-B-A sequences of single source observations, removing signature of linear clock.

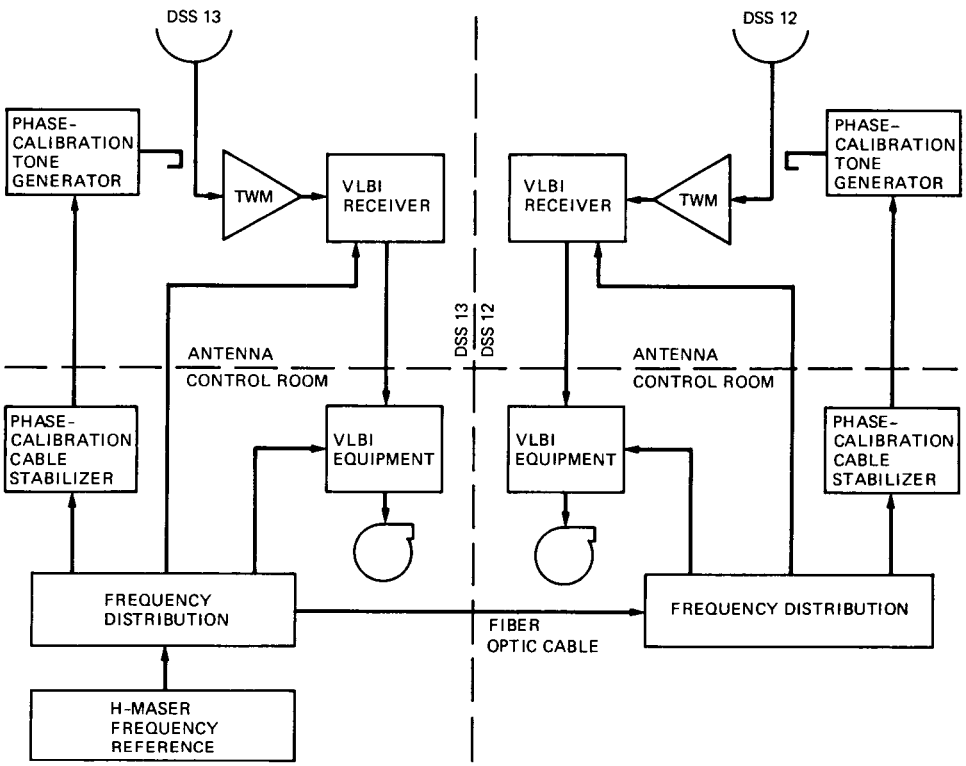

Fig. 1. Experimental configuration for phase delay experiments at Goldstone DSCC. A fiber optic cable transfers a 100-MHz frequency reference from the hydrogen maser at DSS 13 to DSS 12, establishing coherence between the local oscillators at the two stations. Otherwise, the configuration is similar to standard Block 0 VLBI experiments, with data recorded at each station. A full CEI implementation would eliminate the need for data recording, using the fiber optic system for transmission of the observed signals to a common site for real-time correlation.

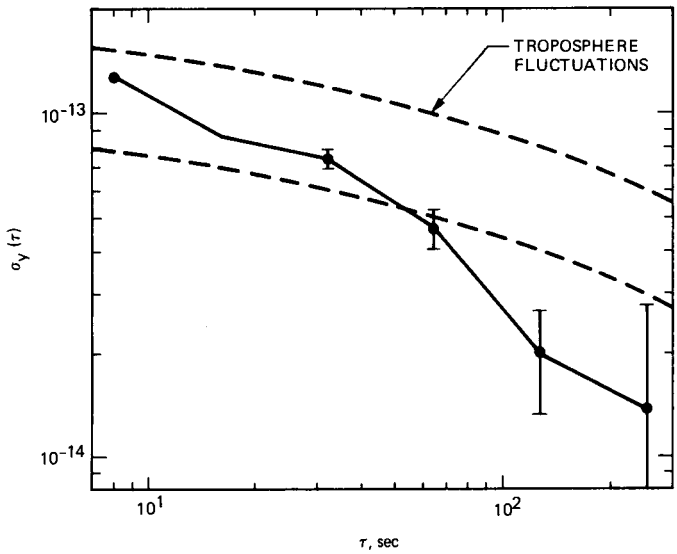

Fig. 2. Allan standard deviation σ_y vs. sample time τ for phase residuals of a 10-minute observation of the bright radio source 3C 84 on the DSS 12-DSS 13 baseline. The dashed lines indicate the range of expected stability due solely to the dynamic wet troposphere, based on a turbulence theory model of water vapor fluctuations. The agreement suggests that such troposphere fluctuations dominate the observed stability, and that the frequency transfer over the fiber optic link is below this level.

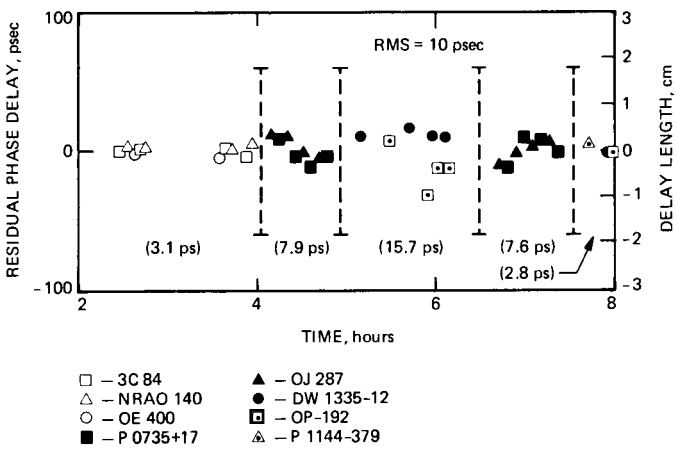

Fig. 3. Phase delay residuals for clusters of 2-3 angularly close radio sources on the DSS 12-DSS 13 baseline. Each source is indicated by a distinct symbol. The vertical dashed lines delimit series of repeated observations for each cluster, and have a height equal to the delay ambiguity at the 8.4-GHz observation frequency. Separate clock offsets were estimated for each series. The RMS scatter for each series is indicated, ranging from 2.8-15.7 psec. The total RMS for all observations is 10 psec.

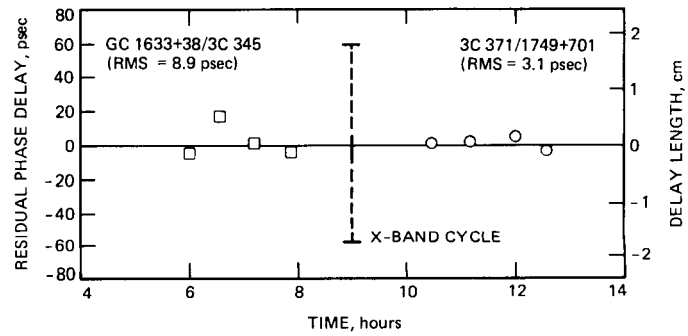

Fig. 4. Differential phase delay residuals for repeated observations of two close quasar pairs, on the 253-km baseline between DSS 13 and the OVRO 40-m antenna. As described in the text, linear combinations are formed for A-B-A observation sequences of each quasar pair to eliminate any linear clock behavior. The total RMS scatter for all eight differential measurements (formed from 24 single source measurements) is 6.7 psec.